Antarctic Geothermal Heat Flow, Crustal Conductivity and Heat Production Inferred From Seismological Data

James A. N. Hazzard[1], **Fred D. Richards**[1]

[1]Department of Earth Science & Engineering, Imperial College London, Royal School of Mines, Prince Consort Road, London, SW7 2AZ, UK

Key Points:

- Demonstration of new methodology for inferring geothermal heat flow from seismological data.
- S- and P-wave velocity used together to infer and fit geotherms.
- Incorporation of laterally varying crustal conductivity and heat production.

Abstract

Geothermal heat flow is a key parameter in governing ice dynamics, via its influence on basal melt and sliding, englacial rheology, and erosion. It is expected to exhibit significant lateral variability across Antarctica. Despite this, surface heat flow derived from Earth's interior remains one of the most poorly constrained parameters controlling ice sheet evolution. To obtain a continent-wide map of Antarctic heat supply at regional-scale resolution, we estimate upper mantle thermomechanical structure directly from V_S. Until now, direct inferences of Antarctic heat supply have assumed constant crustal composition. Here, we explore a range of crustal conductivity and radiogenic heat production values by fitting thermodynamically self-consistent geotherms to their seismically inferred counterparts. Independent estimates of crustal conductivity derived from V_P are integrated to break an observed trade-off between crustal parameters, allowing us to infer Antarctic geothermal heat flow and its associated uncertainty.

Plain Language Summary

The future evolution of the Antarctic Ice Sheet depends on its stability, which describes how sensitive it is to environmental change. A key factor influencing ice sheet stability is how much thermal energy is transferred into its base from Earth's interior: a parameter called geothermal heat flow. If the level of heat supply is high, melting at the base of the ice sheet is encouraged, resulting in enhanced sliding towards outlet glaciers at the continental perimeter. Consequently, ice loss is accelerated, and the likelihood of glacial collapse is increased. Therefore, an accurate map of Antarctic geothermal heat flow, including how this parameter varies from region to region, is needed to produce high quality projections of Antarctic ice mass loss and therefore global sea level change. In this study, we use models of how seismic wave speed varies within Earth to estimate its three-dimensional temperature structure, as well as its thermal conductivity. These data are used to infer a collection of best-fitting models of Earth's thermal state, and hence estimate Antarctic geothermal heat flow.

Corresponding author: James A. N. Hazzard, `j.hazzard20@imperial.ac.uk`

1 Introduction

Heat derived from Earth's interior, and supplied to its surface, is a crucial component of ice sheet basal conditions. The supply of thermal energy to the ice sheet-solid Earth interface can influence basal melt and sliding, englacial rheology, and erosion, and is therefore a key factor in governing ice dynamics (Larour et al., 2012; Burton-Johnson et al., 2020). Not only are ice dynamics highly sensitive to the supply of geothermal heat, the latter is expected to vary significantly across Antarctica (e.g., Shen et al., 2020). The result is that a good understanding of the pattern and amplitude of heat supply into the base of the Antarctic Ice Sheet is a requirement for accurately modelling its evolution.

To quantify heat supply we refer to geothermal heat flow (GHF), q_s, pertaining to the amount of thermal energy supplied across Earth's surface, per unit area and time (units $\mathrm{mW\,m^{-2}}$). Since thermal conduction is the dominant mechanism of heat transfer in Earth's crust, Fourier's law of conduction is used to relate q_s to Earth's temperature structure,

$$\vec{\mathbf{q}}_s = -k(z=z_0)\frac{\partial T}{\partial z}\bigg|_{z=z_0}\hat{\mathbf{z}}, \tag{1}$$

$$q_s = |\vec{\mathbf{q}}_\mathbf{s}|. \tag{2}$$

Here, k is thermal conductivity, T is temperature, z is a locally vertical depth co-ordinate, and z_0 is located at the surface. Theoretically, then, Equation 1 gives us a pathway to estimating q_s, via measurements of laterally varying thermomechanical structure. Indeed, local estimates of Antarctic GHF have been made using observations of temperature and depth from gravity-driven probes in unconsolidated sediment and boreholes drilled into ice or bedrock. However, such measurements can only be used to infer point estimates of GHF.

To obtain continental scale maps of GHF in Antarctica suitable for ice sheet modelling, geophysical methods are an extremely valuable tool. A number of methods based on magnetic, gravity or seismic data have been employed in the past (e.g., An et al., 2015; Martos et al., 2017; Haeger et al., 2022). Whilst useful, such methods have suffered from a range of data- and modelling-derived issues. For example, sparsity of data and a lack of sensitivity to short-wavelength structure has led to poor spatial resolution of inferred GHF models. Poor constraint on crustal parameters such as thermal conductivity and heat production has led to lateral variations being ignored, despite their potential to vary significantly, and the consequent impact of such variations on GHF. Difficulties in converting field observations into estimates of Earth's thermal structure, and the inference of only a single isotherm, has led to large uncertainty in GHF predictions.

A number of recent advances allow for the establishment of a novel approach to infer GHF from seismological data sets. Firstly, the development of ANT-20, a wave-equation traveltime adjoint tomographic model, lays the groundwork for imaging Antarctic thermomechanical structure and henceforth GHF at regional-scale resolution ($\sim$ 100 km) (Lloyd et al., 2020; Hazzard et al., 2023). Secondly, new geochemical analyses have improved our understanding of the likely range of key crustal parameters governing heat supply, their relationship with composition, and to what extent they can be inferred from geophysical data (Jennings et al., 2019; Sammon et al., 2022). Thirdly, the emergence of physics-based parameterisations of mantle rock properties, constrained via laboratory experiments, has opened the door to converting seismic velocities directly into temperature (Faul & Jackson, 2005; Yamauchi & Takei, 2016; Yabe & Hiraga, 2020). In addition, methods to calibrate these parameterisations based on a range of geophysical data constraints have allowed us to reduce uncertainty in such conversions (Richards et al., 2020; Hazzard et al., 2023). Here, we harness the aforementioned advances to produce a new model of Antarctic GHF and its associated uncertainty, based on a new approach integrating both shear- (V_S) and compressional- (V_P) wave velocity data.

2 Methods

Our approach to estimating GHF across Antarctica is motivated by the desire to infer geothermal structure in as direct a fashion as possible, without relying on empirical comparisons to GHF estimates derived from geologically distinct continental environments. Central to this approach is the idea of constraining the relationship between temperature and depth, $T(z)$, across a range of depth slices, rather than relying on a single isotherm. Therefore, we make use of V_S data, which is especially sensitive to geothermal structure throughout the shallow upper mantle. Since crustal composition also plays a key role in determining heat supply, via variations in thermal conductivity and heat production, we seek to constrain these parameters within our modelling framework. To do so, we bring in information from V_P data, which provides sensitivity to lateral variations in $SiO_2\%$ content and therefore crustal conductivity. By fitting steady-state geothermal profiles to V_S-derived counterparts, and looking at how the misfit between the two varies as a function of crustal heat production, we are able to co-constrain conductivity, heat production and geothermal heat flow in a thermodynamically self-consistent fashion. This framework serves as the basis for providing reasonable inferences of q_s.

2.1 Inferring Thermal Structure from Seismic Data

The sensitivity of V_S to temperature (T) derives from the effect that temperature has on the viscoelastic properties of mantle rock. To reliably parameterise the $V_S(T)$ relationship, we adopt the approach of Hazzard et al. (2023), who calibrated the anelasticity parameterisation of Yamauchi & Takei (2016) against a suite of Antarctic geophysical data constraints (see Section S1 for details). Having established a method for relating seismic velocity and temperature, we can select a geographic location $\{\theta, \phi\}$ (longitude, θ, latitude, ϕ) within the spatial footprint of the chosen tomographic model ANT-20, and convert the corresponding radial velocity structure $V_S(z)$ into an inferred geotherm $T(z)$ (Figure 1a, black cross-hairs).

2.2 Fitting Geothermal Profiles

Due to the likely presence of noise and artefacts in the underlying seismic data, as well as the potential for unmodelled compositional seismic velocity variation, we avoid estimating q_s directly from our seismically inferred geotherms. Instead, we fit steady-state, thermodynamically self-consistent geotherms to them. To prepare the V_S-derived geotherms for fitting, we remove crustal velocities, as well as anomalously slow velocities beneath the Mohorovičić discontinuity (Moho) which may be associated with errors in the assumed crustal thickness. We interpolate the resulting geotherms on a 1 km depth interval (see Section S1 for details; Figure 1a, red dashed line).

We fit the geotherms according to a modified version of the procedure laid out in McKenzie et al. (2005). This procedure involves iteratively updating the Moho GHF, and mechanical boundary layer thickness, until the misfit between modelled and V_S-derived geotherms is minimised. Once an optimal geotherm has been arrived at (Figure 1a, black solid line), q_s can be calculated according to the surface temperature gradient and associated thermal conductivity.

2.3 Parameterising Mantle Structure

In addition to providing a seismically inferred geotherm to the fitting procedure, we must also provide a suitable parameterisation for thermal conductivity, k ($\mathrm{W\,m^{-1}\,K^{-1}}$), and heat production, h^* ($\mathrm{\mu W\,m^{-3}}$), in the mantle and crust.

In the mantle, we calculate conductivity according to the temperature- and pressure-dependent parameterisation of Korenaga & Korenaga (2016). We have adapted this pa-

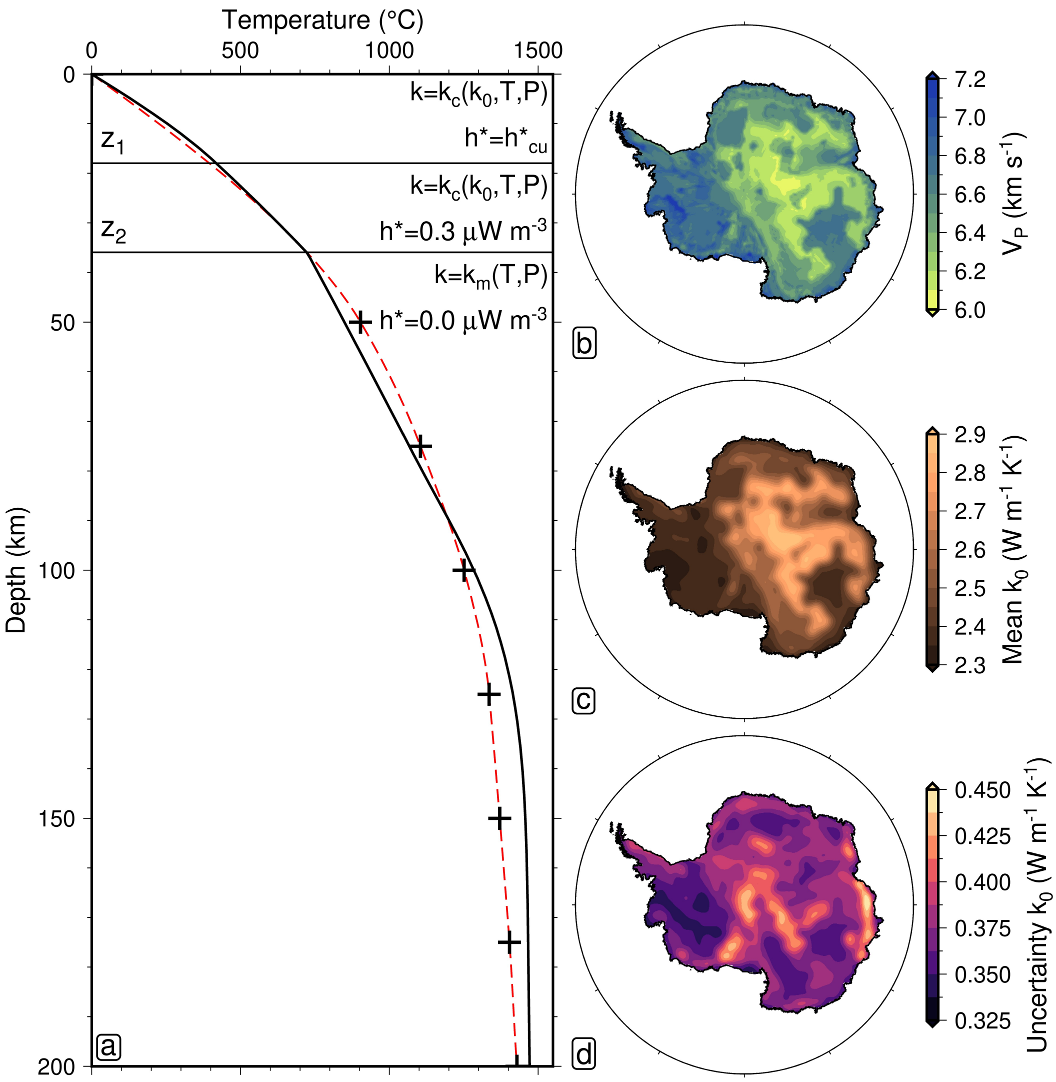

Figure 1. Parameterising Earth structure. (a) Temperature-depth data points inferred from V_S (black cross-hairs) interpolated prior to fitting (red dashed line). Steady-state geotherm fitted to seismic data (black line), subject to depth-dependent thermodynamic constraints within the upper crust ($0 \leq z \leq z_1$), lower crust ($z_1 < z \leq z_2$), and mantle ($z_2 < z$). All depths referenced with respect to the crystalline basement. (b) Average crustal V_P across Antarctica. (c) Crustal conductivity (k_0) estimated from V_P (Equation 4). (d) Uncertainty in k_0 based on spread in crustal V_P and $k_0(V_P)$ residual (Section 2.5).

rameterisation to assume a grain size of 0.1 cm, relevant to the calculation of radiative thermal conductivity. We refer to this parameterisation as $k = k_m(T, P)$. In accordance with the relatively low-abundance of heat-producing elements in the upper mantle, we assume a mantle heat production $h^* = 0.0\,\mu\mathrm{W\,m^{-3}}$. We set constant-pressure heat capacity to $C_P = 1187\ \mathrm{J\,kg^{-1}\,K^{-1}}$, and thermal expansivity to $\alpha = 3 \times 10^{-5}\ \mathrm{K^{-1}}$, in our assumptions of adiabatic mantle properties. We assume a mantle kinematic viscosity of $\nu = 9 \times 10^{16}\ \mathrm{m^2\,s^{-1}}$.

2.4 Parameterising Crustal Structure

To parameterise thermal conductivity in the crust, we make use of the following parameterisation (Goes et al., 2020), which we refer to as $k = k_c(k_0, T, P)$,

$$k_c(k_0, T, P) = \frac{k_0}{n}\,(1 + \beta P)\left(n - 1 + \exp\left[\frac{-(T - 25)}{300}\right]\right). \tag{3}$$

In this equation, the factors $\beta = 0.1$, and $n = 6.4 - 2.3\ln(k_0)$, and k_0 is the reference crustal conductivity at atmospheric conditions ($P = 0$ GPa, $T = 25°$C). Note that this parameterisation was misprinted in the original text of Goes et al. (2020); we have clarified with the authors that the expression above is the correct version.

To parameterise heat production, we divide the crust into two layers of equal depth. We assume a uniformly distributed heat production throughout each layer, set to $h^* = h^*_{\mathrm{cu}}$ in the upper crust, and $h^* = 0.3\,\mu\mathrm{W\,m^{-3}}$ in the lower crust. We have adopted this simple parameterisation to avoid imposing precise details of the depth-dependence of h^* *a priori*, which are not known. When the upper crustal heat production is set to $h^*_{\mathrm{cu}} = 1.0\,\mu\mathrm{W\,m^{-3}}$, our parameterisation is consistent with globally averaged heat production values obtained from a comprehensive analysis of crustal geochemistry and seismic velocity (Sammon et al., 2022).

2.5 Sampling Crustal Parameters to Optimise GHF

Reference thermal conductivity, k_0, and upper crustal heat production, h^*_{cu}, are treated as laterally variable parameters in our model, so as to account for the influence of crustal composition on geothermal structure. Both parameters could exhibit lateral variability within the approximate ranges $k_0 \sim 1.0$ to $4.0\ \mathrm{W\,m^{-1}\,K^{-1}}$ and $h^*_{\mathrm{cu}} \sim 0.0$ to $6.0\ \mu\mathrm{W\,m^{-3}}$ (Hasterok & Chapman, 2011; Jennings et al., 2019; Lösing et al., 2020; Sammon et al., 2022). Such variations can have a significant impact on q_s. For example, we found that for a typical V_S-derived input geotherm, varying k_0 and h^*_{cu} within the aforementioned ranges results in surface GHF variations of $q_s \sim 20$ to $170\ \mathrm{mW\,m^{-2}}$. The lowest (highest) inferred q_s occurs when both k_0 and h^*_{cu} are minimised (maximised). We can rationalise this observation by considering the dependence of q_s on each crustal parameter in turn (see Section S2 for details).

In order to optimise our predictions of GHF at each location, we co-vary k_0 and h^*_{cu}, and evaluate the least-squared misfit between V_S-inferred and fitted geotherms as a function of the two free parameters (Figure 2). If the misfit space at each location were to exhibit a global minimum, this would allow for simultaneous extraction of best-fitting k_0, h^*_{cu} and q_s. However, we find that k_0 and h^*_{cu} trade off significantly with one another. This trade-off can be visualised by holding k_0 constant and varying h^*_{cu}, and vice versa, and observing the similarity in fitted geotherms (Figure 2, panels a-b). Of course, this similarity is also borne out in the misfit space, where we see valley-like minima (Figure 2c). Since q_s trades-off positively with both k_0 and h^*_{cu}, it is vital to be able to locate where in the valley of the misfit space the so-called true solution lies. To resolve this issue and break the observed trade-off, we require additional information, which we obtain by utilising an independent geophysical constraint on k_0.

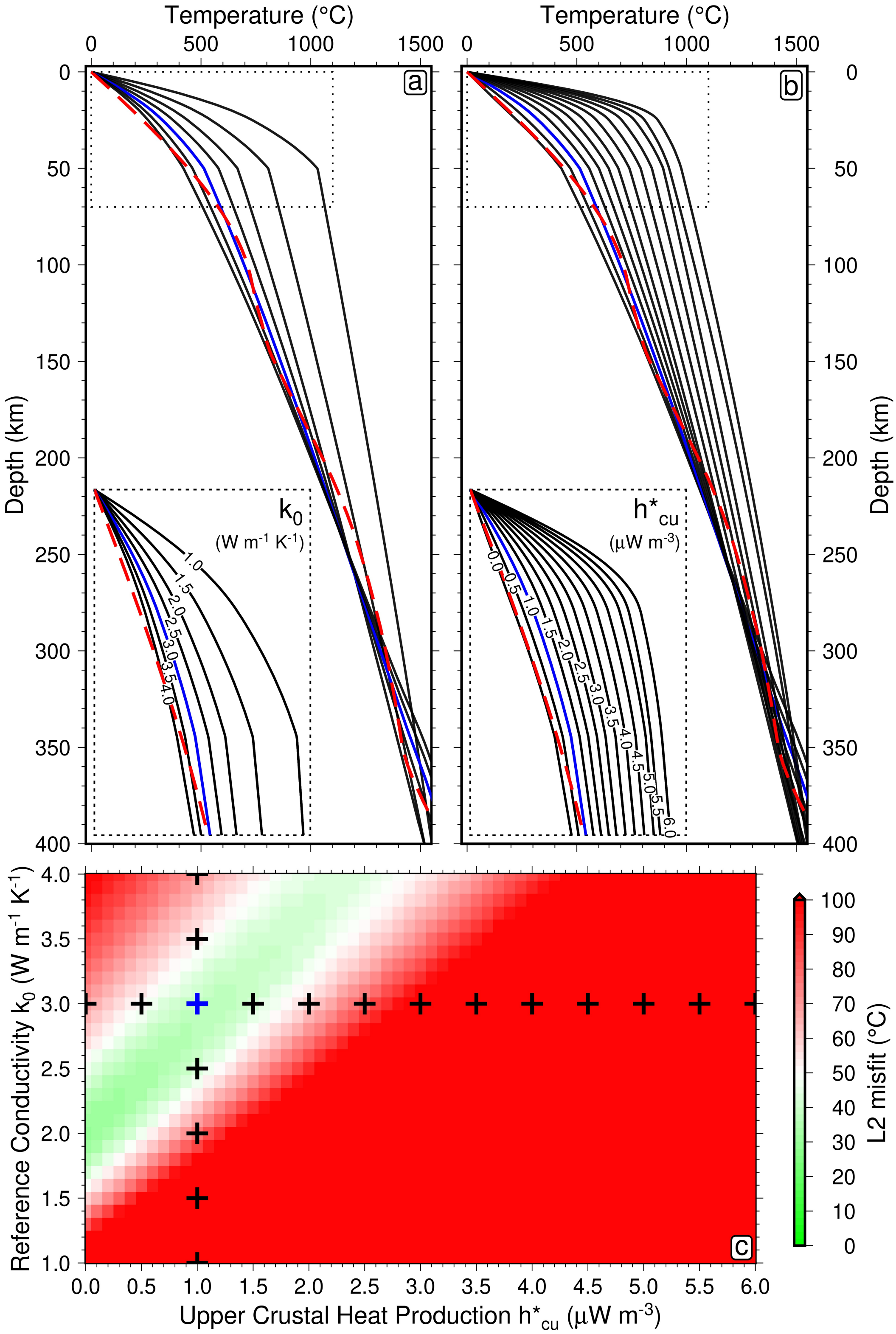

Figure 2. Fitting seismically inferred geotherms. (a) Constant reference conductvity, $k_0 = 2.5\,\mathrm{W\,m^{-1}\,K^{-1}}$, variable upper crustal heat production, h^*_{cu} in range 0.0 to $6.0\,\mathrm{\mu W\,m^{-3}}$. (b) Variable reference conductivity, k_0 in range 1.0 to 4.0 $\mathrm{W\,m^{-1}\,K^{-1}}$, constant upper crustal heat production, $h^*_{cu} = 0.5\,\mathrm{\mu W\,m^{-3}}$. (c) Trade-off between crustal conductivity and upper crustal heat production in misfit between seismically inferred and steady-state fitted geotherm (k_0 and h^*_{cu} combinations used in panels (a) and (b) marked by cross-hairs).

To gain insight into laterally varying crustal conductivity, we draw on a model of crustal V_P ($\mathrm{km\,s^{-1}}$, Figure 1b). We use the same V_P model as was assumed in ANT-20, for consistency with our chosen crustal thickness model. Jennings et al. (2019) relate V_P to k_0 via laboratory measurements on igneous rocks spanning a wide range of compositions. They found that SiO_2 is the dominant control on thermal conductivity. By making use of the empirical relationship,

$$k_0(V_P) = a_0 + a_1 V_P + a_2 V_P^2 \pm \epsilon, \tag{4}$$

$$a_0 = 3.162 \times 10^1 \ \mathrm{W\,m^{-1}\,K^{-1}},$$

$$a_1 = -8.263 \times 10^{-3} \ \mathrm{W\,m^{-2}\,K^{-1}\,s^{-1}},$$

$$a_2 = 5.822 \times 10^{-7} \ \mathrm{W\,m^{-3}\,K^{-1}\,s^{-2}},$$

$$\epsilon = 0.31 \ \mathrm{W\,m^{-1}\,K^{-1}},$$

as provided by Jennings et al. (2019), we estimate Antarctic crustal conductivity by averaging crustal V_P (in $\mathrm{km\,s^{-1}}$) at each continental location, and converting it into k_0 (Figure 1c). In addition, we utilise the spread in V_P data within the crust at each location, along with the $k_0(V_P)$ fitting residual $\epsilon = 0.31 \ \mathrm{W\,m^{-1}\,K^{-1}}$, to estimate an uncertainty in our predicted conductivity (Figure 1d).

Since we now have access to independent predictions of $k_0(\theta, \phi)$ derived from V_P data, we can locate physically plausible regions of k_0-space. We start by sampling a value of k_0 from a Gaussian distribution at each location, according to

$$k_0 \sim \mathcal{N}\left[\mu(k_0), \sigma(k_0)\right], \tag{5}$$

where $\mu(k_0)$ is given by the empirical prediction of equation 9, and $\sigma(k_0)$ is given by the uncertainty associated with this prediction (Figure 1). For each sampled value of k_0, we extract the corresponding best fitting value of h^*_{cu}, as well as the q_s associated with this combination of crustal parameters. By repeating this sampling procedure, we build up a distribution of k_0, h^*_{cu} and q_s. We summarise these distributions at each location using a mean and standard deviation, providing us with Antarctic GHF predictions along with an estimate of their uncertainty.

3 Results and Discussion

3.1 Antarctic GHF Estimates

Resulting estimates of Antarctic GHF are shown in Figure 3. To distinguish between West and East Antarctica, we utilise the satellite-mapped drainage network of Zwally & Giovinetto (2011). Our results indicate high q_s in West Antarctica, where heat supply into the base of the Antarctic Ice Sheet is estimated to vary between 60 and 130 $\mathrm{mW\,m^{-2}}$, and is on average $97\pm14\,\mathrm{mW\,m^{-2}}$ (median, and median absolute deviation, respectively). Such GHF values are significantly higher than the global continental average, $q_s = 67 \pm 47\,\mathrm{mW\,m^{-2}}$ (as inferred from gravity-driven probe and borehole temperature-depth data), and are in fact intermediate between the former and the global average over continental rift zones, $q_s = 114 \pm 94\,\mathrm{mW\,m^{-2}}$ (Lucazeau, 2019). This result is consistent with recent tectonic activity, evidence for Cenozoic magmatism, and inferences of a thermal anomaly beneath West Antarctica (Barletta et al., 2018; Ball et al., 2021; Hazzard et al., 2023). The distribution of q_s values within the aforementioned range is relatively uniform, implying significant lateral heterogeneity across West Antarctica. Maximum q_s is inferred at the continental perimeter in the Amundsen Sea region, and in the northern Antarctic Peninsula.

In East Antarctica, our results indicate q_s in the range 20 to 120 $\mathrm{mW\,m^{-2}}$. Note that the presence of above-continental-average GHF values within this range is indicative of the fact that not all of our defined East Antarctic region is underlain by cold, cratonic material. However, the distribution of inferred GHF is heavily skewed towards lower

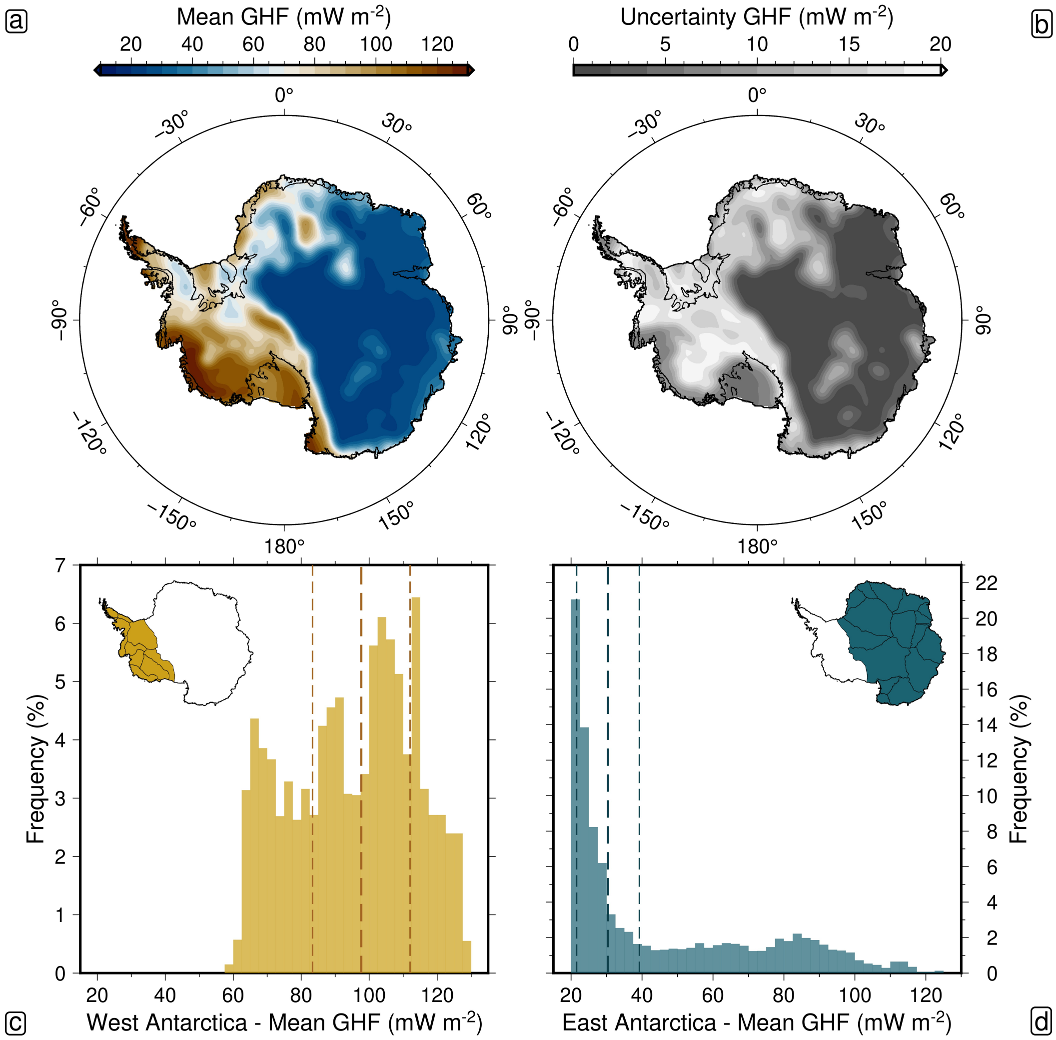

Figure 3. Seismically inferred GHF. (a) Mean. (b) Standard deviation. (c) Distribution over West Antarctica (region defined according to satellite-mapped drainage networks of Zwally & Giovinetto, 2011). (d) Same as (c), East Antarctica.

values, which is borne out in the spatial average 30 ± 8 mW m^{-2}. Such low values are consistent with globally averaged GHF estimates in continental regions of Archean age, $q_s = 46 \pm 21\,\mathrm{mW\,m^{-2}}$ (Lucazeau, 2019).

For the most part, the spatial pattern of GHF uncertainty, $\sigma(q_s)$, is similar to that of the GHF prediction itself, $\mu(q_s)$. The ratio of these two predictions, $\sigma(q_s)/\mu(q_s)$, is on average $16 \pm 10\,\%$ over the Antarctic continent. Elevated proportional uncertainty in GHF structure is estimated in Coats Land and Dronning Maud Land in East Antarctica, in parallel with anomalously high uncertainty in heat production. The least-squared misfit between inferred and modelled geotherm is relatively insensitive to the choice of heat production here, reducing our ability to constrain this parameter and hence q_s. Anomalously low q_s uncertainty ($\sigma(q_s) < 10$ mW m^{-2}) is estimated at the Amundsen Sea Embayment and Ross Ice Shelf, as well as along the grounding line between these two regions. These areas are characterised by high inferred GHF in the region of 100 to $130\,\mathrm{mW\,m^{-2}}$. The uncertainty here is artificially low owing to the inferred heat production lying at the top of the parameter sweep range, $h^*_{\mathrm{cu}} = 6.0\,\mathrm{\mu W\,m^{-3}}$ (see Section S3 for maps of inferred h^*_{cu}). Since the seismically inferred geotherm here is systematically hotter than the modelled profile, the inferred value of h^*_{cu} is insensitive to variations in crustal thermal conductivity, and thus exhibits no variation. We refrain from increasing the upper limit of our parameter sweep in response to this issue, as this would not be an appropriate resolution, since h^*_{cu} values in excess of $6.0\,\mathrm{\mu W\,m^{-3}}$ are inconsistent with the range of physically plausible values based on continental geology (Artemieva et al., 2017; Sammon et al., 2022), and unreasonable increases in h^*_{cu} would be required to attempt to fit the inferred geotherm. Instead, we suggest that the reason for our findings is due to our assumption of a steady-state geotherm. While this assumption is a reasonable approximation across most of Antarctica, it may be less accurate in regions recently affected by intraplate basaltic magmatism or episodes of rifting (e.g., Alexander Island offshore Antarctic Peninsula, Marie Byrd Land and the Victoria Land Basin; LeMasurier, 2008; Sauli et al., 2021). Indeed, by locally modelling time-dependent thermal evolution following lithospheric thinning, we improve fit to V_S-derived temperature in these regions and find that optimal transient geotherms require less extreme h^*_{cu} values than steady-state equivalents (see Section S4 for transient geotherm modelling). Nevertheless, predicted q_s is near-identical for the these two different model assumptions, indicating that, while our steady-state-based prediction likely overestimates h^*_{cu}, our q_s estimates remain valid. Note, however, that uncertainty on q_s is likely higher than predicted in these locations, since the low uncertainty is likely an artefact of the $6.0\,\mathrm{\mu W\,m^{-3}}$ upper limit we impose on upper crustal heat production.

3.2 Comparison With Previous Studies

A comparison of our GHF model with those from previous studies utilising a range of approaches is presented in Figure 4. Consistent across all studies, we observe a long-wavelength pattern of elevated heat supply in West Antarctica, and more uniformly low heat supply in East Antarctica. However, short-wavelength ($\sim 1,000-10,000$ km) structure differs significantly between models (both in terms of spatial pattern, and amplitude), reflecting the range of data sets and modelling assumptions used to construct them. In particular, our model (HR24, Figure 4) spans a significantly greater range ($110\,\mathrm{mW\,m^{-2}}$) than its comparators, with the exception of the two magnetic studies Maule et al. (2005) and Martos et al. (2017), which exhibit exceedingly high peak GHF values of $190\,\mathrm{mW\,m^{-2}}$ and $240\,\mathrm{mW\,m^{-2}}$ respectively. The higher amplitude of GHF variations in this study compared to most models can be explained by our incorporation of laterally heterogeneous crustal composition. In East Antarctica we infer below average crustal heat production, and in West Antarctica we see the opposite; the combined effect of which is to broaden the range of inferred q_s. As compared to a directly analogous model assuming constant $k_0 = 2.5$ W m^{-1} K^{-1} and $h^*_{\mathrm{cu}} = 1.0$ µW m^{-3} (HR23, Figure 4), we predict a 30% in-

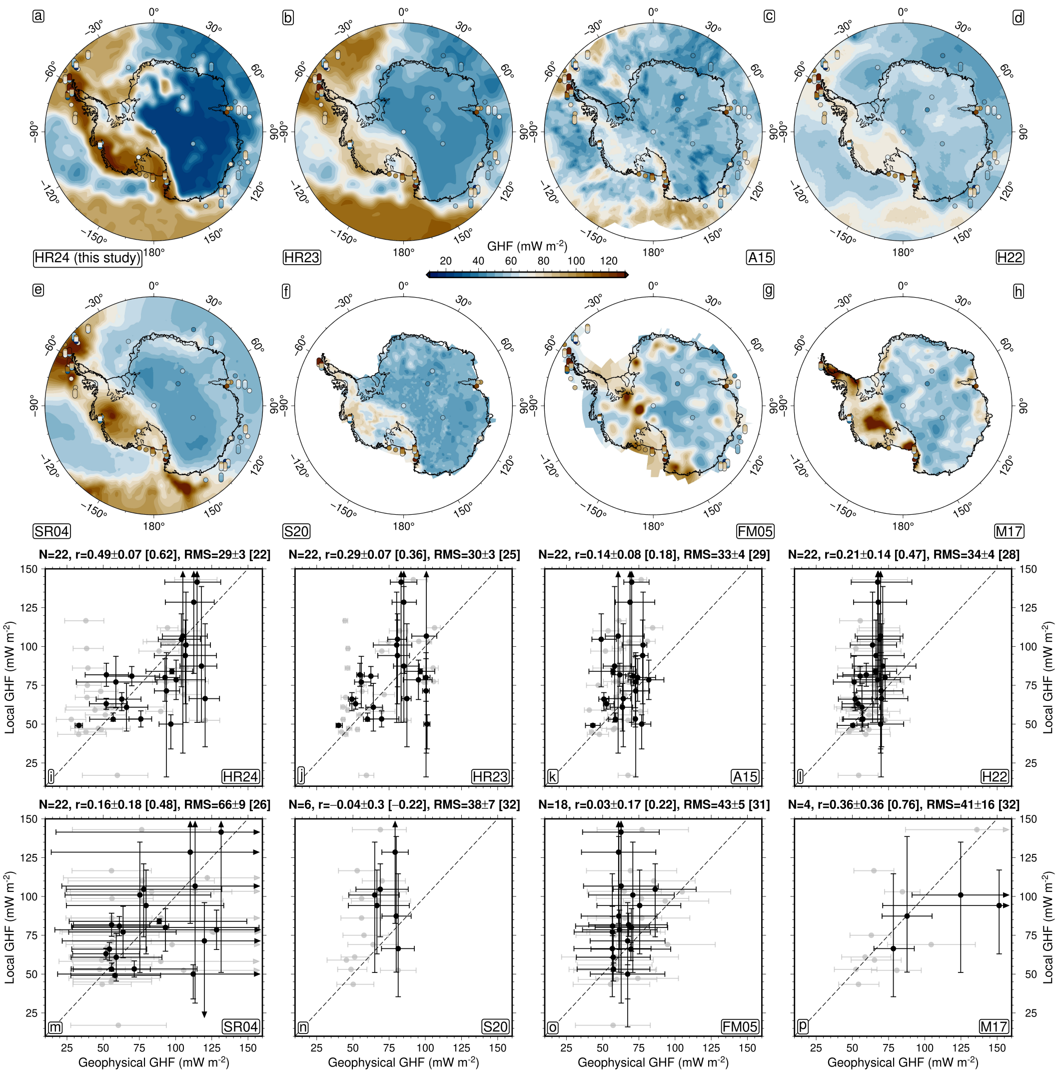

Figure 4. GHF Model Comparison. (a)–(h) Geophysical GHF inferences: HR24 – inferred directly from V_S and V_P (this study); HR23 – inferred directly from V_S (Hazzard et al., 2023); A15 – inferred directly from V_S (An et al., 2015); H22 – inferred via joint seismic and gravity inversion (Haeger et al., 2022); SR04 – inferred empirically via V_S (Shapiro & Ritzwoller, 2004); S20 – inferred empirically via V_S (Shen et al., 2020); FM05 – inferred from magnetic anomaly data (Maule et al., 2005); M17 – inferred from magnetic anomaly data (Martos et al., 2017). GHF inferences derived from gravity-driven probes and boreholes overlain as coloured capsules/circles. Capsules used where 2+ local data points available (coloured by lowest-average-highest local estimate from bottom-middle-top). Circles used where 1 local data point available. Note that HR24 has been extended into the oceanic domain to allow more complete comparison with local data. In the oceanic domain we assume $k_0 = 2.6\ \mathrm{W\,m^{-1}\,K^{-1}}$ and $h^*_{cu} = 0.0\ \mathrm{\mu W\,m^{-3}}$, in keeping with oceanic crustal composition (Grose & Afonso, 2013; Richards et al., 2018). (i)–(p) Relationship between geophysically and locally inferred GHF (Section 3.3), same studies as (a)–(h). Data points and associated error bars show the mean and range of local/geophysical GHF values at each location, respectively. Statistics summarising local-geophysical agreement are: r = Pearson's r-value correlation coefficient; RMS = root-mean-square deviation (values reported in the form a ± b [c], where a=median, b=median absolute deviation, c=value calculated ignoring data uncertainty, see Section S5 for details of analysis). Gray data points correspond to locations where only one local GHF inference is available (i.e., circles in panels (a)–(h)) and are not included in model statistics.

crease in maximum Antarctic q_s, and a 50% reduction in minimum Antarctic q_s (Hazzard et al., 2023).

3.3 Comparison With Local Data

Despite the sparsity of Antarctic GHF estimates derived from in situ temperature probe observations in boreholes and unconsolidated sediment, these data can be utilised to independently assess geophysically informed models of q_s. It is important to treat in situ inferences carefully, since they are representative of localised temperature structure, and are potentially susceptible to contamination by thermal signals caused by frictional heating at the base of the ice sheet, hydrological circulation, and local topography (Shen et al., 2020; Colgan et al., 2021). In addition, limited lateral resolution in our chosen V_S model will smooth out GHF variations on spatial scales smaller than $\sim 100\,\mathrm{km}$, diminishing our ability to accurately compare to local estimates. Therefore, we collect local GHF estimates from gravity-driven probes and boreholes into regions of dimension $100\,\mathrm{km}$, and compare locally and geophysically inferred GHF values in each region (Figure 4). Accounting for data uncertainty in the resulting data sets, our model produces the highest Pearson's correlation coefficient, $\mathrm{r} = 0.49 \pm 0.07$, the lowest root-mean-square deviation, $\mathrm{RMS} = 29 \pm 3\ \mathrm{mW\,m^{-2}}$, and a range of GHF values most consistent with local data (see Section S5 for details of quantitative model comparison). We note that two GHF models frequently used in ice sheet modelling studies, SR04 ($\mathrm{r} = 0.16{\pm}0.18$, $\mathrm{RMS} = 66{\pm}9\ \mathrm{mW\,m^{-2}}$) and FM05 ($\mathrm{r} = 0.03{\pm}0.17$, $\mathrm{RMS} = 43{\pm}5\ \mathrm{mW\,m^{-2}}$) (Shapiro & Ritzwoller, 2004; Maule et al., 2005), perform particularly poorly against independent data as compared to HR24.

3.4 Methodological Appraisal

There are a few reasons why our modelling approach may allow us to arrive at estimates of GHF more consistent with independent data than previous studies. Firstly, the use of a geophysically constrained parameterisation of mantle viscoelasticity enables us to map V_S structure directly into temperature over a range of upper mantle depth slices. This stands in contrast to other studies, such as those based on magnetic data, where only a single isotherm associated with the Curie depth is constrained (Maule et al., 2005; Martos et al., 2017). As a result, more reliable estimates of the geothermal gradient can be made. Secondly, the incorporation of crustal V_P information provides us with sensitivity to lateral variations in thermal conductivity, a parameter which affects q_s both directly via its presence in Equation 1, and to a lesser extent, indirectly via its effect on the geothermal gradient. Thirdly, by combining insights drawn from V_S and V_P data together with thermodynamic models of geothermal structure, we are able to constrain variations in crustal heat production. This stands in contrast to previous studies making use of steady-state geotherm modelling, which have assumed constant composition (An et al., 2015; Haeger et al., 2022; Hazzard et al., 2023). In addition, methods based on empirical comparison of seismic data between continents are unable to account for differences in crustal composition between target and comparison sites (Shapiro & Ritzwoller, 2004; Shen et al., 2020). Therefore, whilst their inferred q_s uncertainty may implicitly capture variations in heat supply associated with crustal composition, their estimates of q_s itself will be agnostic to such variations.

3.5 Outstanding Challenges

Although the GHF modelling framework presented herein provides a powerful method to infer GHF from seismological data, a number of outstanding challenges remain. Chief amongst them is our inability to reliably infer temperature structure from V_S at depths shallower than the Moho. We have mitigated this issue in three ways: by assuming a temperature of $0\ ^\circ\mathrm{C}$ at the crystalline basement, excising anomalous seismic data associated with crustal bleeding, and fitting seismically inferred geotherms using thermodynamically self-consistent models of shallow thermal structure. However, given improved constraints on crustal temperature structure (at vertical resolution of ~ 25 km or higher), it would be possible to generate more reliable predictions of surface geothermal gradient. Such constraints may also help in resolving relative contributions to GHF derived from transient-state geotherms versus crustal heat production. Pn-waves are a type of compressional wave guided along the mantle lid, providing sensitivity to Moho temperature structure. Therefore, a high resolution, continental scale model of Antarctic Pn-velocity (V_{Pn}) would be extremely valuable. Fortunately, this may be on the horizon, with the recent development of a V_{Pn} model of central West Antarctica (Lucas et al., 2021). In general, deployment of additional broadband seismic stations in Antarctica would help to improve the accuracy and spatial resolution of velocity models used to infer geothermal structure.

Secondly, we rely on a parameterisation of geochemical data pertaining to the relationship between k_0 and V_P in order to estimate lateral variations in crustal thermal conductivity (Jennings et al., 2019). This parameterisation inherently assumes that conductivity is sensitive only to silicate content. Further, it assumes that synthetic V_P estimates from thermodynamic calculations on a range of mineral assemblages are accurate, and match up to velocities predicted from real data (Behn & Kelemen, 2003). In reality, systematic errors in modelled V_P associated with the choice of regularisation or starting model will be propagated into systematic errors in predicted k_0. In addition, artefacts in V_P structure caused by data sparsity and the ill-posed nature of the seismic inversion problem may cause us to improperly estimate k_0 at certain locations. Therefore, further validation of methods used to estimate $k_0(V_P)$ are needed.

Finally, the relative sparsity of Antarctic GHF estimates from gravity-driven probes and boreholes presents a clear challenge in assessing the quality of geophysical predictions. A significant expansion of this data set is needed to address the question: what is the most reliable geophysical method for estimating continental GHF? In addition, multiple boreholes at each field sampling region are needed, in order to properly account for localised variations in GHF associated with geology, hydrothermal circulation, and topography (Burton-Johnson et al., 2020). Promisingly, the Rapid Access Ice Drill (RAID) project seeks to address the lack of local data by drilling down to the deepest portions of the Antarctic Ice Sheet (Goodge & Severinghaus, 2016).

4 Conclusions

We have presented a novel modelling framework for estimating GHF from seismological data, incorporating lateral variations in crustal composition. We find that our geophysical inferences of heat supply are in better agreement with local estimates than previous studies, implying that crustal conductivity and heat production act as significant controls on Antarctic heat flow. Our models of Antarctic conductivity, heat production, and GHF provide improved constraints on Antarctic sub-glacial geology and thermal conditions, critical for use in ice sheet modelling studies.

5 Open Research

Figures were prepared using Generic Mapping Tools software. Code and model outputs are available at Hazzard & Richards (2024).

Acknowledgments

JANH acknowledges support from the Natural Environment Research Council (Grant NE/S007415/1). FDR acknowledges support from the Imperial College Research Fellowship Scheme. The authors declare no conflicts of interest relevant to this study. The authors thank the reviewers for their helpful and instructive comments.

References

An, M., Wiens, D. A., Zhao, Y., Feng, M., Nyblade, A., Kanao, M., ... Lévêque, J.-J. (2015, December). Temperature, lithosphere-asthenosphere boundary, and heat flux beneath the antarctic plate inferred from seismic velocities. *J. Geophys. Res. Solid Earth*, *120*(12), 8720–8742. doi: 10/ghz6cw

Artemieva, I. M., Thybo, H., Jakobsen, K., Sørensen, N. K., & Nielsen, L. S. K. (2017). Heat production in granitic rocks: Global analysis based on a new data compilation granite2017. *Earth-Science Reviews*, *172*, 1–26. doi: 10/gsqpr2

Ball, P. W., White, N. J., Maclennan, J., & Stephenson, S. N. (2021). Global influence of mantle temperature and plate thickness on intraplate volcanism. *Nature Communications*, *12*(1), 2045. doi: 10/gsqpr5

Barletta, V. R., Bevis, M., Smith, B. E., Wilson, T., Brown, A., Bordoni, A., ... Wiens, D. A. (2018). Observed rapid bedrock uplift in amundsen sea embayment promotes ice-sheet stability. *Science*, *360*(6395), 1335–1339. doi: 10/gdpc5r

Behn, M. D., & Kelemen, P. B. (2003). Relationship between seismic p-wave velocity and the composition of anhydrous igneous and meta-igneous rocks. *Geochemistry, Geophysics, Geosystems*, *4*(5). doi: 10/bfxd93

Burton-Johnson, A., Dziadek, R., & Martin, C. (2020). Review article: Geothermal heat flow in antarctica: current and future directions. *The Cryosphere*, *14*(11), 3843–3873. doi: 10/gsqpsn

Colgan, W., MacGregor, J. A., Mankoff, K. D., Haagenson, R., Rajaram, H., Martos, Y. M., ... Kjeldsen, K. K. (2021). Topographic correction of geothermal heat flux in greenland and antarctica. *Journal of Geophysical Research: Earth Surface*, *126*(2), e2020JF005598. (e2020JF005598 2020JF005598) doi: 10/gk2783

Faul, U. H., & Jackson, I. (2005). The seismological signature of temperature and grain size variations in the upper mantle. *Earth and Planetary Science Letters*, *234*(1), 119–134. doi: 10.1016/j.epsl.2005.02.008

Faul, U. H., Jackson, I., & X, Y. (2007, April). Diffusion creep of dry, melt-free olivine. *J. Geophys. Res.*, *112*(B4). doi: 10.1029/2006JB004586

Goes, S., Hasterok, D., Schutt, D. L., & Klöcking, M. (2020). Continental lithospheric temperatures: A review. *Physics of the Earth and Planetary Interiors*, *306*, 106509. doi: 10.1016/j.pepi.2020.106509

Goodge, J. W., & Severinghaus, J. P. (2016). Rapid access ice drill: a new tool for exploration of the deep antarctic ice sheets and subglacial geology. *Journal of Glaciology*, *62*(236), 1049–1064. doi: 10.1017/jog.2016.97

Grose, C. J., & Afonso, J. C. (2013). Comprehensive plate models for the thermal evolution of oceanic lithosphere. *Geochemistry, Geophysics, Geosystems*, *14*(9), 3751–3778. doi: https://doi.org/10.1002/ggge.20232

Haeger, C., Petrunin, A. G., & Kaban, M. K. (2022). Geothermal heat flow and thermal structure of the antarctic lithosphere. *Geochemistry, Geophysics, Geosystems*, *23*(10), e2022GC010501. (e2022GC010501 2022GC010501) doi: https://doi.org/10.1029/2022GC010501

Hasterok, D., & Chapman, D. S. (2011). Heat production and geotherms for the continental lithosphere. *Earth and Planetary Science Letters*, *307*(1), 59–70. doi: 10.1016/j.epsl.2011.04.034

Hazzard, J. A. N., & Richards, F. D. (2024). Antarctic geothermal heat flow, crustal conductivity and heat production inferred from seismological data. Retrieved from https://osf.io/54zam (Dataset)

Hazzard, J. A. N., Richards, F. D., Goes, S. D. B., & Roberts, G. G. (2023). Probabilistic assessment of antarctic thermomechanical structure: Impacts on ice sheet stability. *Journal of Geophysical Research: Solid Earth*, *128*(5), e2023JB026653. doi: 10.1029/2023JB026653

Jennings, S., Hasterok, D., & Payne, J. (2019, August). A new compositionally based thermal conductivity model for plutonic rocks. *Geophysical Journal International*, *219*(2), 1377–1394. doi: 10.1093/gji/ggz376

Korenaga, T., & Korenaga, J. (2016). Evolution of young oceanic lithosphere and the meaning of seafloor subsidence rate. *Journal of Geophysical Research: Solid Earth*, *121*(9), 6315–6332. doi: https://doi.org/10.1002/2016JB013395

Larour, E., Morlighem, M., Seroussi, H., Schiermeier, J., & Rignot, E. (2012). Ice flow sensitivity to geothermal heat flux of pine island glacier, antarctica. *Journal of Geophysical Research: Earth Surface*, *117*(F4). doi: https://doi.org/10.1029/2012JF002371

LeMasurier, W. E. (2008). Neogene extension and basin deepening in the west antarctic rift inferred from comparisons with the east african rift and other analogs. *Geology*, *36*(3), 247–250.

Lloyd, A. J., Wiens, D. A., Zhu, H., Tromp, J., Nyblade, A. A., Aster, R. C., … O'Donnell, J. P. (2020). Seismic structure of the antarctic upper mantle imaged with adjoint tomography. *Journal of Geophysical Research: Solid Earth*, *125*(3). doi: 10.1029/2019JB017823

Lucas, E. M., Nyblade, A. A., Lloyd, A. J., Aster, R. C., Wiens, D. A., O'Donnell, J. P., … Huerta, A. D. (2021). Seismicity and pn velocity structure of central west antarctica. *Geochemistry, Geophysics, Geosystems*, *22*(2), e2020GC009471. (e2020GC009471 2020GC009471) doi: https://doi.org/10.1029/2020GC009471

Lucazeau, F. (2019). Analysis and mapping of an updated terrestrial heat flow data set. *Geochemistry, Geophysics, Geosystems*, *20*(8), 4001–4024. doi: https://doi.org/10.1029/2019GC008389

Lösing, M., Ebbing, J., & Szwillus, W. (2020). Geothermal heat flux in antarctica: Assessing models and observations by bayesian inversion. *Frontiers in Earth Science*, *8*. doi: 10.3389/feart.2020.00105

Martos, Y. M., Catalán, M., Jordan, T. A., Golynsky, A., Golynsky, D., Eagles, G., & Vaughan, D. G. (2017). Heat flux distribution of antarctica unveiled. *Geophysical Research Letters*, *44*(22), 11,417-11,426. doi: https://doi.org/10.1002/2017GL075609

Maule, C. F., Purucker, M. E., Olsen, N., & Mosegaard, K. (2005). Heat flux anomalies in antarctica revealed by satellite magnetic data. *Science*, *309*(5733), 464–467. doi: 10/ctwn8p

McCarthy, C., & Takei, Y. (2011, September). Anelasticity and viscosity of partially molten rock analogue: Toward seismic detection of small quantities of melt. *Geophys. Res. Lett.*, *38*(18). doi: 10.1029/2011GL048776

McKenzie, D., Jackson, J., & Priestley, K. (2005). Thermal structure of oceanic and continental lithosphere. *Earth and Planetary Science Letters*, *233*(3), 337–349. doi: https://doi.org/10.1016/j.epsl.2005.02.005

Press, W. H., Teukolsky, S. A., Vetterling, W. T., & Flannery, B. P. (2007). *Numerical recipes: The art of scientific computing* (Third edition ed.). Cambridge University Press.

Richards, F. D., Hoggard, M. J., Cowton, L. R., & White, N. J. (2018). Reassessing the thermal structure of oceanic lithosphere with revised global inventories of basement depths and heat flow measurements. *Journal of Geophysical Research: Solid Earth*, *123*(10), 9136–9161. doi: https://doi.org/10.1029/2018JB015998

Richards, F. D., Hoggard, M. J., White, N., & Ghelichkhan, S. (2020). Quantifying the relationship between short-wavelength dynamic topography and thermomechanical structure of the upper mantle using calibrated parameterization of anelasticity. *Journal of Geophysical Research: Solid Earth*, *125*(9), e2019JB019062. doi: 10.1029/2019JB019062

Sammon, L. G., McDonough, W. F., & Mooney, W. D. (2022). Compositional attributes of the deep continental crust inferred from geochemical and geophysical data. *Journal of Geophysical Research: Solid Earth*, *127*(8), e2022JB024041. (e2022JB024041 2022JB024041) doi: https://doi.org/10.1029/2022JB024041

Sauli, C., Sorlien, C., Busetti, M., De Santis, L., Geletti, R., Wardell, N., & Luyendyk, B. (2021). Neogene development of the terror rift, western ross sea, antarctica. *Geochemistry, Geophysics, Geosystems*, *22*(3), e2020GC009076.

Shapiro, N. M., & Ritzwoller, M. H. (2004). Inferring surface heat flux distributions guided by a global seismic model: particular application to antarctica. *Earth and Planetary Science Letters*, *223*(1), 213–224. doi: 10/fnzhf2

Shen, W., Wiens, D. A., Lloyd, A. J., & Nyblade, A. A. (2020). A geothermal heat flux map of antarctica empirically constrained by seismic structure. *Geophysical Research Letters*, *47*(14), e2020GL086955. (e2020GL086955 2020GL086955) doi: https://doi.org/10.1029/2020GL086955

Takei, Y. (2017). Effects of partial melting on seismic velocity and attenuation: A new insight from experiments. *Annual Review of Earth and Planetary Sciences*, *45*(1), 447–470. doi: 10.1146/annurev-earth-063016-015820

Twinn, G., Riley, T., Fox, M., & Carter, A. (2022). Thermal history of the southern antarctic peninsula during cenozoic oblique subduction. *Journal of the Geological Society*, *179*(6), jgs2022–008.

Yabe, K., & Hiraga, T. (2020). Grain-boundary diffusion creep of olivine: 2. solidus effects and consequences for the viscosity of the oceanic upper mantle. *Journal of Geophysical Research: Solid Earth*, *125*(8). doi: 10.1029/2020JB019416

Yamauchi, H., & Takei, Y. (2016). Polycrystal anelasticity at near-solidus temperatures. *Journal of Geophysical Research: Solid Earth*, *121*(11), 7790–7820. doi: 10.1002/2016JB013316

Zwally, H. J., & Giovinetto, M. B. (2011). Overview and assessment of antarctic ice-sheet mass balance estimates: 1992-2009. *Surveys in Geophysics*, *32*(4), 351–376. doi: 10.1007/s10712-011-9123-5